Inhibitors of trehalose-6-phosphate synthase activity in fungal pathogens compromise thermal tolerance pathways

Yi Miao[a*1], Vikas Yadav[b1], William Shadrick[c^], Jiuyu Liu[c], Alexander R. Jenner[c], Clifford Gee[c@], Martin Schäfer[a%], John R. Perfect[b,d], Richard E. Lee[c], Richard G. Brennan[a#], and Erica J. Washington[a,b#]

[a]Department of Biochemistry, Duke University School of Medicine, Durham, North Carolina, USA

[b]Department of Molecular Genetics and Microbiology, Duke University School of Medicine, Durham, North Carolina, USA

[c]Department of Chemical Biology and Therapeutics, St. Jude Children's Research Hospital, Memphis, Tennessee, USA

[d]Division of Infectious Diseases, Department of Medicine, Duke University School of Medicine, Durham, North Carolina, USA

#Address correspondence to: erica.washington1@duke.edu and richard.brennan@duke.edu

*Present address: Division of Life Science, The Hong Kong University of Science and Technology, Clear Water Bay, Kowloon, Hong Kong SAR, China

^Present address: Incyte Corporation, Wilmington, Delaware

@Present address: Department of Chemistry and Biochemistry, Creighton University, Omaha, Nebraska, USA

%Present address: GCP-Service International Ltd & Co. KG, Bremen, Germany

[1] co-first authors

Running title

Inhibition of fungal trehalose biosynthesis

Keywords: trehalose, Tps1, *Cryptococcus*, *Candida*, antifungal

Abstract

Infections caused by fungal pathogens such as *Candida* and *Cryptococcus* are associated with high mortality rates, partly due to limitations in the current antifungal arsenal. This highlights the need for antifungal drug targets with novel mechanisms of action. The trehalose biosynthesis pathway is a promising antifungal drug target because trehalose biosynthesis is essential for virulence in *Cryptococcus neoformans* and *Candida albicans* and is also a mediator of fungal stress responses, such as thermotolerance. To exploit its untapped antifungal potentials, we screened the St. Jude 3-point pharmacophore library to identify small molecule inhibitors of the first enzyme in the trehalose biosynthesis pathway, trehalose-6-phosphate synthase (Tps1). Structure-guided optimization of a potent hit, SJ6675, yielded a water-soluble inhibitor named 4456dh. Employing biochemical, structural and cell-based assays, we demonstrate that 4456dh inhibits Tps1 enzymatic activity, suppresses trehalose synthesis and exerts a fungicidal effect. Notably, the structure of Tps1 in complex with 4456 reveals that 4456 occupies the substrate binding pocket. Importantly, 4456dh renders normally thermotolerant fungal pathogens unable to survive at elevated temperatures, which is critical as we investigate the emergence of fungi from the environment due to a warming climate. Overall, this work develops the water-soluble 4456dh as an early-stage antifungal drug that has a distinct mechanism of action compared to existing clinical antifungals.

50 **Importance**

51 The rise of fungal infections in recent years is alarming due to an increase in the vulnerable
52 immunocompromised population, global temperature increase and limited antifungal treatment
53 options. One of the major hurdles in developing new drugs is the identification of fungal-specific
54 antifungal drug targets due to highly conserved cellular machinery between fungi and humans.
55 Here, we describe a small molecule inhibitor, 4456dh, of the trehalose biosynthesis pathway. This
56 pathway is present in fungi but not humans. Trehalose plays a critical role in stress responses
57 such as thermotolerance in fungal pathogens and is essential for their virulence. We showed that
58 treatment with 4456dh blocks production of trehalose and renders fungal cells inviable. Thus far,
59 4456dh is active against two fungal pathogens of critical importance suggesting a broad-spectrum
60 activity.

61 **Introduction**

62 The contribution of fungal pathogens to human mortality goes greatly unnoticed compared
63 to that of viruses and bacteria and even other eukaryotic pathogens. Remarkably, the combined
64 mortality associated with fungal pathogens is similar to that caused by malaria and tuberculosis
65 (1). Each year a diverse collection of fungal pathogens cause diseases that result in
66 approximately 6.5 million infections and 2.5 million directly attributable deaths worldwide (2). The
67 World Health Organization recently documented the significance of these fungal pathogens and
68 listed *Cryptococcus neoformans* and *Candida albicans* as critical pathogens, amongst others, and
69 made the call for increased development of antifungal therapeutics, fungal surveillance and
70 diagnostics (3).

71 The current antifungal drug armamentarium consists of polyenes, azoles and
72 echinocandins. While these antifungal drugs have proven to be powerful, they also have
73 drawbacks that include the lack of bioavailability, lack of effectiveness against multiple pathogens
74 and an increase in the likelihood of antifungal drug resistance (4). Current antifungal drugs are
75 also often toxic and require long and difficult treatment regimens (5). Therefore, these drugs are
76 not sufficient to control the current state of fungal infections. Moreover, new fungal pathogens,
77 such as the multidrug-resistant yeast *Candida auris*, are emerging due to changes in the climate
78 (6–11).

79 Because fungi and humans are both eukaryotes, it is difficult yet advantageous to identify
80 an antifungal drug target that is not conserved between both species. An antifungal drug with a
81 target not found in humans is likely to have fewer off-target effects and be less toxic for the
82 immunocompromised patients who are susceptible to invasive fungal infections. Other features
83 of antifungal drugs that are desirable include the possibility of being broad-spectrum in the case
84 of poor diagnostics and a low likelihood that resistance to the antifungal drug will develop.

85 The trehalose biosynthesis pathway in fungal pathogens has been described as a
86 promising antifungal drug target (12). The trehalose biosynthesis pathway is a conserved pathway
87 amongst insects, plants, bacteria and fungi (13). However, the trehalose biosynthesis pathway is
88 not found in mammals (12, 13). Given that the key components of the trehalose biosynthesis
89 pathway are structurally conserved, it may be possible to generate a broad-spectrum antifungal
90 drug that targets this pathway. Attempts have been made to generate compounds that inhibit
91 trehalose biosynthesis in insects (14). Closantel was identified as a potential bioactive molecule
92 that targets the trehalose biosynthesis pathway and has potent activity against *C. neoformans*
93 and *C. gattii in vitro*. However, closantel does not have antifungal activity in murine models (12).

The trehalose biosynthesis pathway in fungal pathogens is a two-step process initiated when trehalose-6-phosphate synthase, Tps1, converts uridine-diphosphate-glucose (UDPG) and glucose-6-phosphate (G6P) to trehalose-6-phosphate (T6P) (15). T6P is dephosphorylated by the trehalose-6-phosphate phosphatase (Tps2) to produce trehalose (15). Some pathogens also contain additional trehalose biosynthesis proteins. For example, in *Aspergillus fumigatus* there are apparently multiple Tps1 enzymes (16). In ascomycetes, including *A. fumigatus*, *C. albicans* and *S. cerevisiae,* there are regulatory trehalose biosynthesis proteins, which lack catalytic activity and are thought to act as scaffolds to enable complex formation of the trehalose biosynthesis proteins (17).

Trehalose is a nonreducing disaccharide composed of two glucose molecules linked by an α,α-1,1-glycosidic bond (α-D-glucopyranosyl-(1→1)-α-D-glucopyranoside). Trehalose is a highly stable molecule that can help proteins and cellular membranes withstand dehydration, salinity, and heat (18–20). Trehalose can also serve as an energy source and is broken down by trehalase into two glucose molecules that funnel into energy-generating pathways such as glycolysis and the pentose phosphate pathway (15, 21, 22). Importantly, the trehalose biosynthesis pathway is strongly associated with virulence in *C. neoformans* and *C. albicans*. In the absence of *TPS1* and *TPS2*, *Cryptococcus* and *Candida* species cannot survive in mammalian hosts (23–27). The contribution of trehalose biosynthesis to thermotolerance in *C. albicans* and *C. neoformans* is critical. Inhibition of trehalose biosynthesis may help control the expansion of thermotolerant environmental isolates, which have the potential to become pathogens.

We now have the tools to take a structure-based approach to developing an inhibitor of Tps1. The recent determination of structures of trehalose biosynthesis proteins from fungal pathogens, including *C. albicans* and *A. fumigatus* has enabled us to utilize a structure-guided approach to designing an inhibitor of trehalose biosynthesis proteins (28, 29). Most recently, cryo-electron microscopy was used to determine detailed binding residues in the *C. neoformans* substrate-binding pocket (30). Tps1 is a GT-B family, retaining glycosyltransferase and contains two catalytic subdomains, connected by a kinked, C-terminal α-helix (31). The N-terminal subdomain binds the sugar acceptor, G6P, and the C-terminal subdomain contains the donor, UDPG. Given that Tps1 utilizes a substrate-assisted mechanism of catalysis, proper alignment of each substrate is required for the formation of T6P. Therefore, targeting the substrate-binding pocket is a critical and facile route to disrupt the function of Tps1. Additionally, the ability to generate large amounts of pure recombinant *C. neoformans* Tps1 and *C. albicans* Tps1 expressed and purified in *E. coli* has made high-throughput compound screens possible.

128 In this work, we developed a fluorescence polarization-based high-throughput screening
129 platform and screened a chemical library containing 750 compounds to identify Tps1 inhibitors.
130 We determined the complex structure of a top hit with cognate *C. albicans* Tps1. Guided by this
131 structural information, we rationally optimized the hit and developed a water-soluble derivative,
132 4456dh. 4456dh demonstrates broad-spectrum inhibitory effects against multiple pathogenic
133 fungal species, including *Candida* and *Cryptococcus*. Furthermore, 4456dh displays temperature-
134 dependent fungicidal activity, phenocopying the *tps1*Δ fungicidal phenotype. Finally, we show that
135 in fungal cells 4456dh inhibits the biosynthesis of trehalose. These data indicate that the
136 mechanism of action of 4456dh is indeed trehalose-dependent and fully exploits the "druggable"
137 thermotolerant characteristics of various pathogenic fungal species.
138 Overall, this work highlights the combination of high-throughput screening, structure-
139 guided hit optimization and cellular assays to develop a promising water-soluble small molecule
140 with desired antifungal properties and the potential for development of a novel antifungal
141 therapeutic.
142

143 **Results**

144 **Seven compounds were identified from a high-throughput screen to inhibit CaTps1 activity**

145 As the first step of the trehalose biosynthesis pathway, Tps1 synthesizes T6P from the
146 substrates UDP-glucose and G6P followed by the release of UDP and T6P (15). To identify a
147 small molecule inhibitor of Tps1 activity, we adapted a high-throughput screen (HTS) utilizing the
148 UDP Transcreener Fluorescence Polarization (FP) assay (32, 33). The FP assay detects the UDP
149 released because of the Tps1-mediated enzymatic reaction (Figure 1A). This highly sensitive HTS
150 has a Z' factor of 0.87, indicating an ideal signal-to-noise ratio. There was a ≥ 175 millipolarization
151 (mP) shift between the positive (free UDP) and negative (cathomycin, also called novobiocin)
152 control in our assay. Recombinant Tps1 from *C. albicans*, hereafter referred to as CaTps1, was
153 expressed in *E. coli* and purified via an N-terminal 6xHis-tag and Ni^{2+}-NTA affinity
154 chromatography, followed by size exclusion chromatography (Figure 1B). A 3-point
155 pharmacophore (3PP) library of 750 compounds of less than 300 Da in molecular mass was
156 screened for the ability to inhibit 6xHis-CaTps1 activity. In the primary screen, 32 (4.2%)
157 compounds that inhibited the activity of 6xHis-CaTps1 by more than 10% at 500 μM concentration
158 were identified (Figure 1C,D). To validate the initial hits, a dose response assay using the same
159 UDP^2 Transcreener FP assay was performed (Supplemental Figure 1). At the completion of the
160 screen, seven compounds that inhibit the activity of CaTps1 were selected for further investigation
161 (Figure 1E and Table 1).

162 **Generation of a library of derivatives of SJ6675**

163 We initiated a structure-guided approach to generate derivatives of the compounds by
164 attempting *de novo* co-crystallization of each of the seven compounds with CaTps1. We
165 successfully obtained a 3.5 Å resolution structure of SJ6675 ((4-furan-3-yl)thiazol-2-amine) in
166 complex with CaTps1 (Supplemental Figure 2A and Supplemental Table 1). This structure
167 revealed the presence of SJ6675 in the substrate-binding pocket of CaTps1 (Supplemental Figure
168 2A), proximal to conserved substrate-binding residues R280, K285, N382 and L383 (28). These
169 data indicate that SJ6675 likely interferes competitively with the binding of the UDPG substrate.

170 We designed a library of SJ6675 derivatives and tested the derivatives for inhibition of
171 CaTps1 activity (Supplemental Figure 2B,C). Many of the compounds, diluted in DMSO,
172 precipitated when added to the Tps1 activity assay reaction and several of the compounds
173 increased the activity of CaTps1 (Supplemental Figure 2C). However, one of these compounds,
174 4456, significantly inhibited the activity of CaTps1 and did not precipitate in the assay solution
175 (Supplemental Figure 2C).

176

177 **4456dh binds Tps1 with high affinity and inhibits the Tps1-mediated release of UDP**

178 To determine the ability to use 4456 as a lead compound using biochemical approaches,
179 we generated a water-soluble derivative of 4456, which we shall now refer to as 4456dh, for 4456-
180 dichloride hydrate (Figure 2A). The composition of 4456dh was confirmed by NMR and elemental
181 analysis (Supplemental Figure 3).

182 Thermal shift assays were completed to determine if 4456dh binds Tps1. We
183 hypothesized that the binding of 4456dh to Tps1 would increase Tps1 stability, resulting in a
184 higher melting temperature. Therefore, CaTps1 and *C. neoformans* Tps1, hereafter referred to as
185 CnTps1, were incubated with 4456dh overnight at 4 °C. Glo-Melt dye was added to the mixture
186 prior to determining the thermostability. Surprisingly, we observed that 4456dh decreased the
187 melting temperature of both CaTps1 and CnTps1 in thermal shift assays indicating a
188 destabilization of the Tps1 enzyme upon binding (Figure 2B,C). These data indicate that 4456dh
189 binds to both *C. albicans* Tps1 and *C. neoformans* Tps1 but again leads to destabilization of the
190 Tps1 enzyme.

191 To determine the binding affinity of 4456dh and CaTps1 and CnTps1, microscale
192 thermophoresis (MST) was used. Given their intrinsic fluorescence, we were able to detect
193 binding without the use of additional fluorophores. MST experiments revealed that the binding
194 affinities of 4456dh with recombinant 6xHis-CaTps1 and 6xHis-CnTps1 are 7.1 μM and 33.4 μM,
195 respectively (Figure 2D,E). These binding affinities are consistent with the concentration of
196 4456dh at which we can detect a shift in Tps1 stability in the thermal shift assays.

197 The ability of 4456dh to inhibit the activity of CaTps1 was tested using a
198 spectrophotometric-coupled Tps1 enzyme assay, in which recombinant 6xHis-CaTps1 was
199 incubated with 1 mM 4456dh at 4 °C for 16 hours. The activity of 6xHis-CaTps1 was determined
200 by determining the initial rate of the reaction. The activity of 6xHis-CaTps1 was reduced
201 approximately 30% in the presence of 4456dh (Figure 2F). Similarly, the effect of 1 mM 4456dh
202 on 6xHis-CnTps1 activity was determined. 4456dh inhibited the activity of 6xHis-CnTps1 activity
203 by approximately 30% (Figure 2G). Therefore, 4456dh directly binds and inhibits the activity of
204 Tps1 from *C. albicans* and *C. neoformans*.

205 **4456dh binds the substrate-binding pocket of CaTps1**

206 To gain insight into the mode of action of 4456dh, we grew crystals of 6xHis-tagged *C.*
207 *albicans* Tps1 (6xHis-CaTps1) in complex with 4456 and determined the structure to 3.35 Å

208 resolution (Figure 3A and Table 2). The structure of the 6xHis-CaTps1-4456 complex was solved
209 using molecular replacement and the structure of CaTps1 bound to UDP and G6P (PDB: 5HUU),
210 with UDP and G6P removed as the search query. The final model of the 6xHis-CaTps1-4456
211 complex consists of N-terminal and C-terminal subdomains consisting of residues 6 to 239 and
212 246 to 437, respectively, followed by the C-terminal α-helix (Figure 3A). The final model also
213 contains one 4456 molecule per subunit of 6xHis-CaTps1 (Figure 3A,B).

214 During refinement, electron density corresponding to 4456 was identified in the substrate-
215 binding pocket of CaTps1 between the N-terminal G6P-binding lobe and the C-terminal UDPG-
216 binding lobe. Polder omit maps of the bound inhibitor show the binding of 4456 (Supplemental
217 Figure 4). 4456 was modelled into the electron density between these two lobes and was found
218 to make contacts with multiple conserved residues in the substrate-binding pocket, including
219 critical substrate-binding residues (Figure 3C and Supplemental Figure 5) (28). The conserved
220 residues near 4456 are also proximal to the native product, UDP, and substrate G6P (Figure 3D).
221 The model of the catalytic modified-Rossman fold domains and the C-terminal α-helix is
222 structurally similar to previously determined structures of Tps1 from *C. neoformans*, *A. fumigatus*
223 and *E. coli,* and therefore, demonstrate the likelihood that 4456 also binds in the conserved
224 catalytic pockets of Tps1 from these additional organisms (Supplemental Figure 6A) (28, 30).
225 Using a ConSurf analysis, the degree of conservation was mapped onto Tps1 structures and
226 revealed that the most highly conserved residues are either buried in the substrate-binding pocket
227 or are proximal to that region (Supplemental Figure 6B) (34). This finding was expected given that
228 4456 is a derivative of a lead compound that also binds the substrate-binding pocket of CaTps1
229 (Supplemental Figure 2).

230 **4456dh is bioactive against *Candida* and *Cryptococcus* cells**

231 We tested the effects of 4456dh on live cells by determining the minimal inhibitory
232 concentrations (MICs) of these compounds. Following the standard Clinical and Lab Standards
233 Institute (CLSI) MIC broth microdilution methods, wild-type *C. albicans* SC5314 was grown with
234 4456dh in the yeast-peptone-dextrose (YPD) medium at 42 °C for 48 hours (Figure 4A). The
235 concentration of 4456dh ranged from 10 μM to 13 mM. 4456dh inhibited the growth of *C. albicans*
236 at 42 °C with an MIC of 4.8 mM, whereas no MIC was detected at 30 °C (Figure 4A and
237 Supplemental Figure 7A). We characterized the fungicidal activity of 4456dh by growing the *C.*
238 *albicans* on compound-free YPD plates after exposure to 4456dh. We observed temperature-
239 dependent fungicidal activity of 4456dh on *C. albicans* at 42 °C (Figure 4A and Supplemental
240 Figure 7B).

241 Further, we determined the effect of 4456dh on the growth of *C. auris* B11220. We
242 performed MIC assays at 39 °C and determined that 4456dh inhibited the growth of *C. auris* with
243 an MIC of 3.5 mM at 39 °C (Figure 4A). The MIC increased at 30 °C to 18 mM (Supplemental
244 Figure 7A). Fungicidal activity of 4456dh on *C. auris* was also detected at both 30 °C and 39 °C
245 (Figure 5A and Supplemental Figure 7B).

246 4456dh displayed the most potent activity on *C. glabrata*, with an MIC of 7.5 μM at 42 °C
247 (Figure 4B). Furthermore, there was significant fungicidal activity of 4456dh on *C. glabrata* in
248 concentrations ranging from 7.8 μM to 500 μM (Figure 4B). The activity against *C. glabrata* was
249 specific to 42 °C, as no MIC or fungicidal activity was detected at 30 °C (Supplemental Figure
250 7A,B).

251 We next tested the activity of 4456dh on *Crypotococcus* species at 37 °C (Figure 4C)
252 using concentrations of 4456dh ranging from 10 μM to 13 mM. We found that 4456dh inhibited
253 the growth of *C. neoformans*, *C. deneoformans*, and *C. gattii* with MIC of 5.6 mM, 0.5 mM, and
254 7.0 mM, respectively (Figure 4C). Fungicidal activity of 4456dh was also detected in all the
255 *Cryptococcus* species tested at 37 °C (Figure 4C). Interestingly, 4456dh also displayed fungicidal
256 activity on *C. deneoformans* at 30 °C at 13 mM (Supplemental Figure 7C).

257 The activity of 4456dh at 30 °C was an indicator that there is at least one other target of
258 4456dh, in addition to Tps1. To test this hypothesis, we performed zone of inhibition studies in
259 the *C. deneoformans* background (Supplemental Figure 8A). In these assays a lawn of cells was
260 spread onto plates containing YPD medium. A sterile disc soaked with either water, 1 μg/mL
261 FK506 as a positive control, or 4456dh was placed on the media and the effect of the growth of
262 *C. deneoformans* was observed after 2 days at the indicated temperatures (35). At 37 °C, there
263 was a distinct zone of inhibition surrounding 4456dh (Supplemental Figure 8A). Consistent with
264 our prediction of an additional target of 4456dh, we detected a diffuse, yet visible zone of inhibition
265 due to 4456dh on *C. deneoformans tps1*Δ cells (Supplemental Figure 8B).

266 **4456dh inhibits trehalose biosynthesis in cells**

267 Given that 4456dh inhibits the activity of CaTps1 and CnTps1 *in vitro* and has bioactivity
268 against multiple *Candida* and *Cryptococcus* species, we next aimed to determine whether 4456dh
269 affects trehalose production in cells. To test this hypothesis, we quantified trehalose levels in cells
270 treated with 4456dh at sub-lethal concentrations as determined by the MIC assays using a
271 colorimetric spectrophotometric assay. We measured trehalose production in wild-type *C.*
272 *albicans* at 30 °C and 42 °C, in the presence and absence of 4456dh. We observed that at 30 °C,

273 there was a minimal amount of trehalose detected and, therefore, there was no significant change
274 detected in the presence of 4456dh (Figure 5A). However, we observed a significant increase in
275 trehalose content when *C. albicans* was exposed to high temperature stress ($P < 0.0001$; Figure
276 5A). The addition of 0.5 mM 4456dh to *C. albicans* at 42 °C, resulted in an approximate two-fold
277 decrease in trehalose content (Figure 5A).

278 Similarly, we observed an increase in trehalose accumulation in *C. neoformans* cells
279 grown at 37 °C, compared to 30 °C (Figure 5B). Treatment of *C. neoformans* with a sublethal
280 dose of 4456dh at 37 °C resulted in a significant decrease in trehalose ($P < 0.05$; Figure 5B).
281 These data are consistent with our hypothesis that 4456dh disrupts the substrate-binding
282 capability of Tps1 and, therefore, prevents trehalose biosynthesis.

283 **Discussion**

284 Fungal pathogens are causing large devastation to the ecosphere ranging from
285 agriculturally important crops to amphibians, bats and humans. These invasive fungal infections
286 are prevalent worldwide and are responsible for millions of mortalities each year. To curb this
287 significant rate of disease and death, the development of the antifungal arsenal needs to be
288 continued and expanded to address concerns with antifungal drug resistance and the emergence
289 of new fungal pathogens due to many factors, including climate change.

290 Here we have focused on the development of a lead compound that targets Tps1 from *C.*
291 *albicans* and *C. neoformans*, two predominant pathogenic fungal species in the clinics (1, 36).
292 They have been highlighted as critical pathogens by the World Health Organization (3). Tps1 is a
293 key enzyme in the critical first step of the trehalose biosynthesis pathway (15). Tps1 is a
294 glycosyltransferase enzyme that uses substrates UDPG and G6P to generate the intermediate,
295 trehalose-6-phosphate (T6P), which also acts as a signalling molecule. Tps1 is required for
296 growth at 37 °C, capsule formation and growth on glucose in *C. neoformans* and *C. gattii* (24, 25,
297 37). *C. albicans* Tps1 also contributes to pathogenesis-related factors such as biofilm formation
298 and hyphal transition from yeast (28). Perhaps most importantly, trehalose accumulates to high
299 levels upon exposure of *Candida* and *Cryptococcus* to heat stress (24, 25). Tps1 is required for
300 this response. Understanding this molecular mechanism and how to thwart it are critical to our
301 complete understanding of how these fungal pathogens can survive at the elevated body
302 temperature of the human host and cause disease.

303 4456dh is a derivative of a lead compound identified in a screen to identify inhibitors of
304 CaTps1 catalytic activity. We determined, using orthogonal methods, including microscale
305 thermophoresis, thermal shift assays, a spectrophotometrically-coupled enzyme assay and x-ray
306 crystallography, that 456dh binds and competitively inhibits the activity of Tps1 (Supplemental
307 Figure 9). Thus, 4456dh has bioactivity against a broad range of *Candida* and *Cryptococcus*
308 species (Figure 4). Additionally, 4456dh also blocks the heat stress-induced hyperaccumulation
309 of trehalose in both *C. albicans* and *C. neoformans* (Figure 5).

310 We also discovered that 4456dh may have an additional target. Given that it is a small
311 molecular weight compound, and GT-B glycosyltransferases have structurally conserved folds, it
312 is not surprising. We hypothesize that 4456dh may target another glycosyltransferase and predict
313 that it is one that does not involve a temperature-responsive phenotype because 4456dh retains
314 partial activity at 30 °C in a *C. deneoformans tps1*Δ mutant. We identified multiple proteins in *C.*
315 *albicans* and *C. neoformans* with structural similarity to Tps1 that may be affected by treatment

316 with 4456dh (Supplemental Figure 10 and Supplemental Tables 2 - 4). Future work will be needed
317 to identify and characterize the additional target amongst these and other proteins.

318 There were great differences in the potency of 4456dh against fungal species. 4456dh
319 minimal inhibitory concentration values were the lowest for *C. glabrata*, reaching 7.5 μM, whilst
320 the other MICs were in the millimolar range for the fungi tested (Figure 4). We were not able to
321 find a clear structural explanation for the differences, given the significant conservation of the
322 residues and structures of the substrate-binding pockets of Tps1 enzymes for these organisms
323 (Supplemental Figures 5,6). Therefore, we hypothesize that the ability of 4456dh to enter the cell
324 may underly the range of potency of 4456dh or the differences in the activity of 4456dh may also
325 be due to the presence of a secondary protein target amongst the *Candida* and *Cryptococcus*. In
326 the future, we aim to identify the additional target, or targets, of 4456dh using a directed, *in silico*
327 approach to model 4456dh into glycosyltransferases in *Candida* and *Cryptococcus*. We shall also
328 pursue a chemical genomics approach to determining targets of 4456dh.

329 Additional future structure-activity relationship studies using 4456dh will benefit from our
330 initial structure of 4456dh bound to CaTps1. This scaffold, in addition to the previous structures
331 of Tps1 will make generation of derivatives of 4456dh a more facile approach to improving the
332 compound into a more Tps1-targeted drug. Our future studies will also include improving the
333 selectivity of 4456dh, as well as the determination of the toxicity of 4456dh. We expect low toxicity
334 in mammalian subjects, from 4456dh, given that the trehalose biosynthesis pathway is not found
335 in mammals. However, any additional target of 4456 may result in potential toxic effects. Our use
336 of medicinal chemistry to synthesize new derivatives of 4456dh can result in a more soluble,
337 potent and Tps1-specific compound.

338 Importantly, in this report, we have provided proof of principle for successful
339 pharmacological inhibition of Tps1, an enzyme in the trehalose biosynthesis pathway, which is
340 central to fungal pathogen virulence and thermotolerance.

341

342 **Methods and Materials**

343 **Strains**

344 Fungal strains used in this study are listed in Supplemental Table 5. Strains were stored as
345 glycerol stocks at -80 °C. Strains were grown at 30 °C on YPD (1% yeast extract, 2% Bacto
346 Peptone, 2% dextrose) agar plates.

347 **Synthesis of N-(4-(1-methyl-1H-pyrazol-4-yl)thiazol-2-yl)-2-(pyridin-2-yl)acetamide**
348 **Dichloride Hydrate(4456).**

349 To a stirred solution of 4-(1-methyl-1H-pyrazol-4-yl)thiazol-2-amine (**1,** 1.75 g, 9.71 mmol) in dry
350 DMF (20mL) at room temperature, a single portion of 2-(pyridin-2-yl)acetic acid hydrochloride (**2**,
351 3.71 g, 21.36 mmol) and HBTU (8.10 g, 21.36 mmol) was added. The resulting mixture was stirred
352 at room temperature for 5 minutes, followed by the addition of DIPEA (5.59 g, 48.50 mmol). The
353 reaction was stirred for 1 hour before being partitioned between dichloromethane and water. The
354 organic layer was washed with brine, dried over Na_2SO_4 and the solvent was removed under
355 reduced pressure. The residue was redissolved in ethyl acetate (EA), and a pale solid was
356 obtained by filtration (1.25g, 43.0%). To convert the product to its dichloride form, 20 mL of 1M
357 HCl in MeOH was added to the suspended solution of **4456** (1.25g) in MeOH. Once the
358 suspending solution became clear, the solvent was evaporated, and the residue was treated with
359 EA. The solid was collected by filtration as **4456** dichloride hydrate (1.66g, 100%). ^{1}H NMR (400
360 MHz, D_2O) δ 8.81 (dd, J = 6.3, 1.7 Hz, 1H), 8.61 (td, J = 8.0, 1.6 Hz, 1H), 8.12 – 7.87 (m, 4H),
361 7.18 (s, 1H), 3.92 (s, 3H), 3.35 (s, 2H). Anal. Calcd for $C_{14}H_{13}N_5OS$ H_2O 2.2HCl: C 42.29, H 4.36,
362 N 17.62, Cl 19.62; Found C 42.52, H 4.53, N 17.33, Cl 19.46.

363 **Chemistry**

364 4-(1-methyl-1H-pyrazol-4-yl)thiazol-2-amine (**1**) was purchased from Enamine. ^{1}H NMR spectra
365 were recorded on a Bruker 400 MHz NMR spectrometer. Chemical shifts (δ) are reported in parts
366 per million relative to the residual solvent peak or internal standard (tetramethylsilane) and
367 coupling constants (J) are reported in hertz (Hz). The purity of the products was confirmed by
368 UPLC/MS (the Waters Acquity). Elemental analysis was tested by Atlantic Microlab Inc.

369 **Expression and Purification of *C. albicans* Tps1**

370 *C. albicans* Tps1 (CaTps1) was purified as previously described (28). Briefly, the full-length *TPS1*
371 gene from *C. albicans* strain SC5314 was codon-optimized for expression in *E. coli* (Genscript)
372 and cloned into the pET-28a vector, which contains an N-terminal 6xHis affinity tag followed by a
373 thrombin cleavage site. The construct was transformed into BL21(DE3)pLysS cells (Life
374 Technologies, Inc.) and induced with 0.5 mM isopropyl β-D-1-thiogalactopyranoside (IPTG) at 15
375 °C overnight. Supernatants from lysed cultures were loaded onto a nickel column (Ni-NTA,
376 Qiagen) and washed in a buffer containing 50 mM Tris-HCl pH 8.0, 300 mM NaCl, 5 mM $MgCl_2$,
377 5% glycerol and 5 mM imidazole. The protein was eluted with increasing amounts of imidazole in
378 the wash buffer. The fractions containing 6xHis-CaTps1 were pooled, reduced to 5 mL and
379 purified further using S200 size exclusion column chromatography (HiLoad 26/600 Superdex
380 200pg, Cytiva) in a precooled buffer containing 20 mM Tris-HCl pH 8.0, 200 mM NaCl, 5% glycerol
381 and 1 mM β-mercaptoethanol. 5 mL fractions from the size exclusion column containing 6xHis-
382 CaTps1, as determined by SDS-PAGE analysis, were pooled and concentrated using 30K MWCO
383 Amicon Ultra concentrators (Millipore) to 1 mg/mL for downstream applications.

384 **Expression and Purification of *C. neoformans* Tps1**

385 *C. neoformans* Tps1 (CnTps1) was purified as previously described (30). Briefly, the full-length
386 *TPS1* gene from *C. neoformans* strain H99 was codon-optimized for expression in *E. coli*
387 (Genscript) and subcloned using ligation-independent cloning into pMCSG7 (38). The construct

388 was transformed into *E. coli* OverExpress C41(DE3) chemically competent cells engineered for
389 high protein expression (Sigma). Supernatants from lysed cultures, induced with 0.5 mM isopropyl
390 β-D-1-thiogalactopyranoside (IPTG), were loaded onto a nickel column (Ni-NTA, Qiagen) and
391 washed in a buffer containing 50 mM Tris-HCl pH 8.0, 300 mM NaCl, 5 mM $MgCl_2$, 5% glycerol
392 and 5 mM imidazole. The protein was eluted with increasing amounts of imidazole in the wash
393 buffer. The fractions containing 6xHis-CnTps1 were pooled, reduced to 5 mL and purified further
394 using S200 size exclusion column chromatography (HiLoad 26/600 Superdex 200pg, Cytiva)
395 using a precooled buffer containing 20 mM Tris-HCl pH 8.0, 300 mM NaCl, 5% glycerol and 2 mM
396 β-mercaptoethanol. 5 mL fractions from the size exclusion column containing 6xHis-CnTps1, as
397 determined by SDS-PAGE analysis, were pooled and concentrated to 1 mg/mL for downstream
398 applications.

399 **Microscale Thermophoresis Assays**

400 Recombinant and 6xHis-taggged CaTps1 and CnTps1 were purified according to the procedures
401 described above. CaTps1 and CnTps1 were diluted to 5 µM in buffer containing (SEC buffer with
402 0.05% Tween20). For the dilution series, a 100 µM solution of 4456dh was prepared using the
403 same buffer. The stock solution was used for the 16-step serial dilution in the buffer, with a final
404 volume of 10 µL of 4456dh in each reaction mixture of the dilution series. 10 µL of protein was
405 added to the 16 vials and samples were mixed by pipetting up and down. Reactions were
406 incubated overnight at room temperature. Samples were loaded into Monolith NT LabelFree
407 Premium capillaries. MST was performed at Medium MST power for both CaTps1 and CnTps1.
408 The data were acquired with MO.Control 1.5.3 (NanoTemper Technologies GmbH). Recorded
409 data were analyzed with MO.Affinity Analysis 2.2.7 (NanoTemper Technologies GmbH). The MST
410 on-time that yielded that highest signal-to-noise ratio was used for the K_d determination, where
411 K_d is the equilibrium dissociation constant.

412 **Thermal Shift Assays**

413 6xHis-CaTps1 and 6xHis-CnTps1 (2 µM) were individually incubated with 4456dh (100 µM) in 20
414 mM Tris-HCl pH 8.0, 300 mM NaCl, 5% glycerol and 2 mM β-mercaptoethanol buffer containing
415 2X Glo-melt dye. Thermal denaturation was measured using an RT-PCR thermocycler (BioRad)
416 between 25 °C and 95 °C at 0.5 °C increments. The melting temperatures of each sample were
417 determined by identifying the inflection point of the derivative data.

418 **Tps1 Enzyme Activity Assay**

419 The catalytic activity of *C. albicans* Tps1 and *C. neoformans* Tps1 was measured via a continuous
420 enzyme-coupled assay as previously reported (39). Briefly, either 6xHis-CaTps1 or 6xHis-CnTps1
421 were concentrated in a buffer containing 20 mM Tris-HCl pH 8.0, 300 mM NaCl, 5% glycerol and
422 2 mM β-mercaptoethanol. The assay was performed in an assay buffer containing 50 mM HEPES
423 pH 7.8, 100 mM KCl, 5 mM $MgCl_2$ and 2 mM DTT. Final concentrations of 3 µM protein were
424 combined with 1 mM UDPG and 1 mM G6P. Activity assays were performed in clear, flat-
425 bottomed 96-well microtiter plates and the decrease in absorbance at 340 nm was recorded using
426 a plate reader (Tecan). The decrease in absorbance was analyzed for the first 200s of the kinetic
427 reaction.

428 ***De novo* co-crystallization and structure determination of *C. albicans* Tps1-4456 complex**

429 *C. albicans* Tps1 (6xHis-CaTps1) in SEC buffer (20 mM Tris-HCl pH 8.0, 200 mM NaCl, 5%
430 glycerol and 1 mM β-mercaptoethanol) was concentrated to 25 mg/mL using Amicon Ultra
431 concentrators (30 MWCO, Millipore). 4456 which was added to the crystallization drop to a final
432 concentration of 10 mM, from a 100 mM stock solution dissolved in 100% DMSO. Crystals were
433 grown at 25 °C by hanging-drop vapor diffusion methods. Diffraction-quality crystals appeared
434 after 3-4 days in a mother liquor solution containing 0.2 M magnesium sulfate, 0.1 M Tris-HCl pH

435 8.5 and 40% polyethylene glycol (PEG) 400. The crystals were cryo-preserved by looping and
436 dipping a crystal for 1-2 seconds in a solution containing the crystallization reagent supplemented
437 with 25% (v/v) glycerol. Data were collected at the Advanced Light Source (ALS) beamline 5.0.2
438 and processed with XDS (40). The structure of *C. albicans* Tps1-4456 was determined by
439 molecular replacement using the *C. albicans* Tps1-UDP-G6P complex (PDB 5HUU, (28)) as the
440 search model after removal of the UDP and G6P. Iterative cycles of model building were done in
441 COOT (41) and refinement using Phenix refine. Selected data collection and refinement statistics
442 are listed in Table 2.

443 **Minimum Inhibitory Concentration Assay**

444 Wild-type *C. albicans* strains SC5314, wild-type *C. glabrata* CBS138 and wild-type *C. auris*
445 B11220 were cultured overnight in YPD (yeast-peptone-dextrose) medium at 30 °C. Growth of
446 the overnight cultures was quantified by measuring the OD_{600} and corrected for the background
447 absorbance of the medium. Antifungal potency for 4456dh was assessed by minimum inhibitory
448 concentration (MIC) dose-response assays performed under standard Clinical and Lab Standards
449 Institute (CLSI) conditions. A volume of 125 µL from each diluted cell suspension was dispensed
450 into the wells of 96-well flat-bottom microtiter plates (Corning). An additional 25 µL of 4456dh from
451 a series of dilutions from the 157 mM stock solution prepared in water was added to each well.
452 Following preparation, the plates were incubated at the either 30 °C or 42 °C, as indicated, for 48
453 hours. All dose-response assays were performed in biological triplicate with a minimum of three
454 technical replicates. Growth, as determined by a reading of absorbance at 600 nm, was
455 normalized to untreated controls and was corrected for the absorbance of 4456dh in the YPD
456 medium. Growth was plotted as a heat map using Excel.

457 Wild-type *C. neoformans* strains H99, wild-type *C. deneoformans* JEC21 and wild-type *C. gattii*
458 R265 were cultured overnight in YPD (yeast-peptone-dextrose) medium at 30 °C. Growth of the
459 overnight cultures was quantified by measuring the OD_{600} and corrected for the background
460 absorbance of the medium. Antifungal potency for 4456dh was assessed by minimum inhibitory
461 concentration (MIC) dose-response assays performed under standard Clinical and Lab Standards
462 Institute (CLSI) conditions. A volume of 125 µL from each cell suspension was dispensed into the
463 wells of 96-well flat-bottom microtiter plates (Corning). An additional 25 µL of 4456dh from a series
464 of dilutions from the 157 mM stock solution prepared in water was added to each well. Following
465 preparation, the plates were incubated at the either 30 °C or 37 °C, as indicated, for 72 hours. All
466 dose-response assays were performed in biological triplicate with a minimum of three technical
467 replicates. Growth, as determined by a reading of absorbance at 600 nm, was normalized to
468 untreated controls and was corrected for the absorbance of 4456dh in the YPD medium. Growth
469 was plotted as a heat map using Excel.

470 **Fungicidal Assays**

471 Cells previously exposed to compounds for 48 or 72 hours in dose-response matrices were
472 spotted to test the viability of treated cells. 3 µL was extracted from each well with a multi-channel
473 pipette and dispensed onto drug-free YPD agar plates. Plates were incubated at 30 °C for 48
474 hours and photographed. All experiments were performed in biological and technical duplicate.

475 **Trehalose Measurement**

476 *Candida* and *Cryptococcus* strains were grown in liquid cultures at 30 °C and then 42 °C or 37
477 °C, respectively. Cells at each temperature were exposed to either water (vehicle control) or 0.5
478 mM 4456dh. The OD_{600} was determined followed by dilution of overnight cultures to an equivalent
479 of 0.1 OD_{600} of cells. Cells were pelleted, frozen and lyophilized and stored in -80 °C. Pellets were
480 lysed by vortexing with sterile glass beads. The cell-free extract was generated by adding 1X PBS
481 and centrifuging the tubes to pellet the glass beads. The supernatant containing cell-free extracts

482 was exposed to trehalase (Sigma) overnight at 37 °C and then tested for trehalose levels
483 according to the Glucose Assay Kit (MAK476, Sigma) protocol.

484 **Zone of Inhibition Assays**

485 Strains were grown in overnight cultures in YPD (yeast-peptone-dextrose) medium at 30 °C.
486 Optical density (OD_{600}) was determined with an Infinite PRO plate reader (Tecan). OD_{600} was
487 adjusted to 0.01 (10^6 cells/mL) through dilution with YPD, and 200 µL diluted culture from each
488 strain was plated onto YPD plates and spread using sterile beads (Sigma). After the plates had
489 dried, a single disk soaked with either 15 µL of water, 4456dh or 1 µg/mL FK506 disk (6 mm
490 diameter, Becton, Dickinson and Company) was placed in a quadrant of each plate. Plates were
491 incubated at either 30 °C or 37 °C for 48 h and then imaged.

Acknowledgements

E.J.W is supported by the Duke Science and Technology Initiative. This work was also funded by grant 1P01AI104533 from the US NIH to R.G.B., R.E.L., and J.R.P. J.R.P. is also supported by grants AI73896 and A193257.

We thank all current and past Washington laboratory members for helpful discussions, as well as all current and past Brennan laboratory members. We are grateful to Dr. Jennifer Tenor for helpful discussions of the manuscript and Dr. Joseph Heitman for critical reading of the manuscript. We thank Angela Rivera, former graduate student in the Heitman laboratory, for assistance in minimum inhibitory concentration pilot experiments. We thank Natalie Schulte of the Duke University Department of Chemistry and Dr. Peter Silinski, Director of the Department of Chemistry Shared Instrument Facility for training and access to microscale thermophoresis instrumentation.

We thank the Advanced Light Source for access to 5.0.2. beamline. The Berkeley Center for Structural Biology is supported by the Howard Hughes Medical Institute, Participating Research Team members, and the National Institutes of Health, National Institute of General Medical Sciences, ALS-ENABLE grant P30 GM124169. The Advanced Light Source is a Department of Energy Office of Science User Facility under Contract No. DE-AC02-05CH11231.

Y.M., V.Y., W.S. and E.J.W. conducted most experiments, and interpreted data and results. C.G., J.L., A.J. and M.S. conducted some experiments and interpreted data and results. E.J.W. wrote the original draft of the manuscript. E.J.W., R.E.L., R.G.B and J.R.P. conceived the study and interpreted data and results and assisted with editing the manuscript.

Data Availability

Atomic models of CaTps1-SJ6675 and CaTps1-4456 have been deposited in the RCSB Protein Data Bank (PDB) (https://rcsb.org) with accession codes PDB ID 9NKB and PDB ID 9NIQ, respectively. All additional data, including raw data and images associated with all figures, is available upon reasonable request to R.G.B. and E.J.W., the corresponding authors.

520 **Figure Legends**

521 **Figure 1. Seven Tps1 inhibitors were identified using a high-throughput fluorescence**
522 **polarization screen. A)** Diagram of the Transcreener assay for Tps1 activity. **B)** Coomassie-
523 stained SDS polyacrylamide gel of purified recombinant 6xHis-CaTps1. Molecular weight markers
524 are shown with the 50 kDa protein standard highlighted with an arrow. **C)** Pipeline and results
525 from the Tps1 UDP Transcreener assay. **D)** Dot plot of % inhibition and compounds that were
526 tested for inhibition of 6xHis-CaTps1 activity. The 32 compounds above 10% inhibition at 500 μM
527 are highlighted. **E)** The chemical structures and identities of validated 6xHis-CaTps1-inhibiting hit
528 compounds. The compound SJ6675 used in additional studies is boxed.
529

530 **Figure 2. 4456dh binds Tps1 and inhibits Tps1 activity. A)** Structure of 4456dh. **B-C)** Glo-melt
531 thermal shift assays reveal 4456dh destabilizes 6xHis-CaTps1 (B) and 6xHis-CnTps1 (C). The
532 first derivative of the raw data was used to determine the melting temperature of 1 μM 6xHis-
533 CaTps1 (B) and 1 μM 6xHis-CnTps1 (C) treated without or with 2 mM 4456dh. **D-E)** Microscale
534 thermophoresis assays demonstrate 4456dh binds to 6xHis-CaTps1 (D) and 6xHis-CnTps1 (E)
535 with indicated K_d. The top panel shows a representative of the MST trace with the cold region
536 labeled highlighted in blue and the hot region highlighted in red. The bottom panel shows the
537 dose-response curve. The resulting dose-response curves were fitted to a one-site binding model
538 to extract K_d values; the standard deviation was calculated using the K_d values from each
539 independent experiment (n=3). **F)** Tps1 enzyme activity assay with 5 μM 6xHis-CaTps1 (F) and
540 6xHis-CnTps1 (G) +/- 1 mM 4456dh. Error bars represent standard error. Comparison to control,
541 untreated 6xHis-CaTps1, was performed using Student's t-test; $^{**}p < 0.01$, $^{***}p < 0.001$.
542

543 **Figure 3. Structure of *C. albicans* Tps1 in complex with 4456. A)** Structure of one subunit of
544 the CaTps1-4456 complex shown as a surface rendering. **B)** 4456 is found in the deep cavity of
545 the substrate-binding pocket proximal to known substrate-binding residues. **C)** Tps1 residues
546 within 4 Å of 4456 are labelled, shown as stick representations and indigo colored. **D)** Residues
547 within 4 Å of 4456 are proximal to residues that also interact with product and substrate, UDP and
548 G6P (atom-colored sticks), in the CaTps1-UDP-G6P complex (PDB: 5HUU) (28).
549

550 **Figure 4. 4456dh inhibits the growth of *Candida* and *Cryptococcus* species.** Two-fold dose
551 response assays were performed against **A)** *C. albicans* at 42 °C and *C. auris* at 39 °C, **B)** *C.*
552 *glabrata* at 42 °C, and **C)** *C. neoformans*, *C. deneoformans* and *C. gattii* at 37 °C. 4456dh was
553 administered at the concentrations indicated. Cultures were grown in YPD at the listed
554 temperatures for 48 hours for *Candida* species and 72 hours for *Cryptococcus* species. (Left)
555 Relative growth of treated samples was calculated by averaging technical triplicates and
556 normalizing the OD_{600} of each treated well to the average OD_{600} of the untreated wild-type
557 controls, after the absorbance due to the compound was subtracted. (Right) Spot assays show
558 the ability of cells to grow after exposure to 4456dh and indicate fungicidal activity of 4456dh.
559

560 **Figure 5. 4456dh treatment results in reduced trehalose accumulation.** Trehalose
561 accumulation measurements for *C. albicans* **(A)** and *C. neoformans* **(B)** cultured at indicated
562 temperatures in the absence or presence of 0.5 mM 4456dh. Trehalose was measured using a
563 colorimetric glucose assay after treatment of cultures with trehalase. Statistical comparisons were
564 done with a one-way ANOVA analysis followed by a posthoc Tukey's test. Error bars represent
565 standard error.
566

567 **Tables**

568 **Table 1. Small molecules identified in high-throughput screen that inhibit the activity of**
569 **6xHis-CaTps1.**

570

Compound	Chemical Formula	Molecular Weight	CaTps1 FP (% inhibition)	CaTps1 Inhibition Assay (μM)
SJ000805629-1	$C_7H_5NO_2$	135.12	32.19	685.4
SJ000866675-1	$C_7H_6N_2OS$	166.20	13.69	983.3
SJ000866077-1	$C_8H_{13}NO_3S$	203.26	11.12	1231.5
SJ000866063-1	$C_{10}H_{11}ClN_2$	194.66	18.96	767.5
SJ000866107-1	$C_{11}H_{13}ClN_2$	208.69	18.24	1152.3
SJ000866390-1	$C_{10}H_{13}N_3$	175.24	36.36	608.7
SJ000866536-1	$C_9H_{16}N_2O$	168.24	18.64	546.9

571

572

573 **Table 2. Data collection and refinement statistics of structure of 6xHis-CaTps1 in**
574 **complex with 4456.**
575

6xHisCaTps1 – 4456 complex	
Resolution range	58.78 - 3.35 (3.47 - 3.35)
Space group	P 6_4 2 2
Unit cell	117.6 117.6 134.0 90 90 120
Total reflections	75,865 (7,778)
Unique reflections	7,644 (753)
Multiplicity	9.9 (10.3)
Completeness (%)	91.66 (94.0)
Mean I/sigma(I)	14.9 (3.3)
Wilson B-factor	78.7
R-merge	0.1037 (0.2833)
R-meas	0.1089 (0.297)
R-pim	0.03209 (0.08654)
$CC_{1/2}$	0.998 (0.932)
CC*	0.999 (0.982)
Reflections used in refinement	7641 (753)
Reflections used for R-free	716 (71)
R-work	0.2504 (0.3147)
R-free	0.2893 (0.3509)
Number of non-hydrogen atoms	3644
macromolecules	3623
ligands	21
solvent	0
Protein residues	456
RMS(bonds)	0.003
RMS(angles)	0.53
Ramachandran favored (%)	94.9
Ramachandran allowed (%)	4.45
Ramachandran outliers (%)	0.67
Rotamer outliers (%)	0.00
Clashscore	5.12
Average B-factor	83.35
macromolecules	83.25
ligands	100.62

576 Statistics for the highest-resolution shell are shown in parentheses.
577

578 **References**

579 1. Brown GD, Denning DW, Gow NAR, Levitz SM, Netea MG, White TC. 2012. Hidden killers:
580 human fungal infections. Sci Transl Med 4:165rv13.

581 2. Denning DW. 2024. Global incidence and mortality of severe fungal disease. Lancet Infect
582 Dis S1473-3099(23)00692–8.

583 3. 2022. WHO Fungal Priority Pathogens List to Guide Research, Development and Public
584 Health Action. World Health Organization, Geneva.

585 4. Puumala E, Fallah S, Robbins N, Cowen LE. 2024. Advancements and challenges in
586 antifungal therapeutic development. Clin Microbiol Rev 37:e0014223.

587 5. May RC, Stone NRH, Wiesner DL, Bicanic T, Nielsen K. 2016. *Cryptococcus*: from
588 environmental saprophyte to global pathogen. Nature Reviews Microbiology 14:106–117.

589 6. Nnadi NE, Carter DA. 2021. Climate change and the emergence of fungal pathogens. PLoS
590 Pathog 17:e1009503.

591 7. Garcia-Solache MA, Casadevall A. 2010. Global warming will bring new fungal diseases for
592 mammals. mBio 1:e00061-10.

593 8. Casadevall A. 2020. Climate change brings the specter of new infectious diseases. J Clin
594 Invest 130:553–555.

595 9. Casadevall A, Kontoyiannis DP, Robert V. 2019. On the Emergence of *Candida auris*:
596 Climate Change, Azoles, Swamps, and Birds. mBio 10.

597 10. Chaabane F, Graf A, Jequier L, Coste AT. 2019. Review on Antifungal Resistance
598 Mechanisms in the Emerging Pathogen *Candida auris*. Frontiers in Microbiology 10:2788.

599 11. Casadevall A, Kontoyiannis DP, Robert V. 2021. Environmental *Candida auris* and the
600 Global Warming Emergence Hypothesis. mBio 12:e00360-21.

601 12. Perfect JR, Tenor JL, Miao Y, Brennan RG. 2017. Trehalose pathway as an antifungal target.
602 Virulence 8:143–149.

603 13. Gancedo C, Flores C-L. 2004. The importance of a functional trehalose biosynthetic pathway
604 for the life of yeasts and fungi. FEMS Yeast Res 4:351–359.

605 14. Kern C, Wolf C, Bender F, Berger M, Noack S, Schmalz S, Ilg T. 2012. Trehalose-6-
606 phosphate synthase from the cat flea *Ctenocephalides felis* and *Drosophila melanogaster*:
607 gene identification, cloning, heterologous functional expression and identification of
608 inhibitors by high throughput screening. Insect Mol Biol 21:456–471.

609 15. Thammahong A, Puttikamonkul S, Perfect JR, Brennan RG, Cramer RA. 2017. Central Role
610 of the Trehalose Biosynthesis Pathway in the Pathogenesis of Human Fungal Infections:
611 Opportunities and Challenges for Therapeutic Development. Microbiol Mol Biol Rev 81.

612 16. Al-Bader N, Vanier G, Liu H, Gravelat FN, Urb M, Hoareau CM-Q, Campoli P, Chabot J,
613 Filler SG, Sheppard DC. 2010. Role of trehalose biosynthesis in *Aspergillus fumigatus*
614 development, stress response, and virulence. Infect Immun 78:3007–3018.

615 17. Bell W, Sun W, Hohmann S, Wera S, Reinders A, De Virgilio C, Wiemken A, Thevelein JM.
616 1998. Composition and functional analysis of the *Saccharomyces cerevisiae* trehalose
617 synthase complex. J Biol Chem 273:33311–33319.

618 18. Elliott B, Haltiwanger RS, Futcher B. 1996. Synergy between trehalose and Hsp104 for
619 thermotolerance in *Saccharomyces cerevisiae*. Genetics 144:923–933.

620 19. Singer MA, Lindquist S. 1998. Thermotolerance in *Saccharomyces cerevisiae*: the Yin and
621 Yang of trehalose. Trends Biotechnol 16:460–468.

622 20. Tapia H, Young L, Fox D, Bertozzi CR, Koshland D. 2015. Increasing intracellular trehalose
623 is sufficient to confer desiccation tolerance to *Saccharomyces cerevisiae*. Proc Natl Acad
624 Sci U S A 112:6122–6127.

625 21. Meikle AJ, Chudek JA, Reed RH, Gadd GM. 1991. Natural abundance ^{13}C-nuclear magnetic
626 resonance spectroscopic analysis of acyclic polyol and trehalose accumulation by several
627 yeast species in response to salt stress. FEMS Microbiol Lett 66:163–167.

628 22. Crowe JH, Crowe LM, Chapman D. 1984. Preservation of membranes in anhydrobiotic
629 organisms: the role of trehalose. Science 223:701–703.

630 23. Zaragoza O, Blazquez MA, Gancedo C. 1998. Disruption of the *Candida albicans* TPS1
631 gene encoding trehalose-6-phosphate synthase impairs formation of hyphae and decreases
632 infectivity. J Bacteriol 180:3809–3815.

633 24. Ngamskulrungroj P, Himmelreich U, Breger JA, Wilson C, Chayakulkeeree M,
634 Krockenberger MB, Malik R, Daniel H-M, Toffaletti D, Djordjevic JT, Mylonakis E, Meyer W,
635 Perfect JR. 2009. The trehalose synthesis pathway is an integral part of the virulence
636 composite for *Cryptococcus gattii*. Infect Immun 77:4584–4596.

637 25. Petzold EW, Himmelreich U, Mylonakis E, Rude T, Toffaletti D, Cox GM, Miller JL, Perfect
638 JR. 2006. Characterization and regulation of the trehalose synthesis pathway and its
639 importance in the pathogenicity of *Cryptococcus neoformans*. Infect Immun 74:5877–5887.

640 26. Martínez-Esparza M, Martínez-Vicente E, González-Párraga P, Ros JM, García-Peñarrubia
641 P, Argüelles J-C. 2009. Role of trehalose-6P phosphatase (TPS2) in stress tolerance and
642 resistance to macrophage killing in *Candida albicans*. Int J Med Microbiol 299:453–464.

643 27. Van Dijck P, De Rop L, Szlufcik K, Van Ael E, Thevelein JM. 2002. Disruption of the *Candida*
644 *albicans* TPS2 gene encoding trehalose-6-phosphate phosphatase decreases infectivity
645 without affecting hypha formation. Infect Immun 70:1772–1782.

646 28. Miao Y, Tenor JL, Toffaletti DL, Maskarinec SA, Liu J, Lee RE, Perfect JR, Brennan RG.
647 2017. Structural and In Vivo Studies on Trehalose-6-Phosphate Synthase from Pathogenic
648 Fungi Provide Insights into Its Catalytic Mechanism, Biological Necessity, and Potential for
649 Novel Antifungal Drug Design. mBio 8.

650 29. Miao Y, Tenor JL, Toffaletti DL, Washington EJ, Liu J, Shadrick WR, Schumacher MA, Lee
651 RE, Perfect JR, Brennan RG. 2016. Structures of trehalose-6-phosphate phosphatase from
652 pathogenic fungi reveal the mechanisms of substrate recognition and catalysis. Proc Natl
653 Acad Sci U S A 113:7148–7153.

654 30. Washington EJ, Zhou Y, Hsu AL, Petrovich M, Tenor JL, Toffaletti DL, Guan Z, Perfect JR,
655 Borgnia MJ, Bartesaghi A, Brennan RG. 2024. Structures of trehalose-6-phosphate
656 synthase, Tps1, from the fungal pathogen *Cryptococcus neoformans*: A target for
657 antifungals. Proc Natl Acad Sci U S A 121:e2314087121.

658 31. Breton C, Snajdrová L, Jeanneau C, Koca J, Imberty A. 2006. Structures and mechanisms
659 of glycosyltransferases. Glycobiology 16:29R-37R.

660 32. Owicki JC. 2000. Fluorescence Polarization and Anisotropy in High Throughput Screening:
661 Perspectives and Primer. Journal of Biomolecular Screening 5:297–306.

662 33. Lowery RG, Kleman-Leyer K. 2006. Transcreener™: screening enzymes involved in
663 covalent regulation. Expert Opinion on Therapeutic Targets 10:179–190.

664 34. Glaser F, Pupko T, Paz I, Bell RE, Bechor-Shental D, Martz E, Ben-Tal N. 2003. ConSurf:
665 identification of functional regions in proteins by surface-mapping of phylogenetic
666 information. Bioinformatics 19:163–164.

667 35. Lee Y, Lee K-T, Lee SJ, Beom JY, Hwangbo A, Jung JA, Song MC, Yoo YJ, Kang SH,
668 Averette AF, Heitman J, Yoon YJ, Cheong E, Bahn Y-S. 2018. *In Vitro* and *In Vivo*
669 Assessment of FK506 Analogs as Novel Antifungal Drug Candidates. Antimicrob Agents
670 Chemother 62.

671 36. Fisher MC. 2012. Emerging fungal threats to animal, plant and ecosystem health. Nature
672 484.

673 37. Goughenour K, Creech A, Xu J, He X, Hissong R, Giamberardino C, Tenor J, Toffaletti D,
674 Perfect J, Olszewski M. 2024. *Cryptococcus neoformans* trehalose-6-phosphate synthase
675 (tps1) promotes organ-specific virulence and fungal protection against multiple lines of host
676 defenses. Front Cell Infect Microbiol 14:1392015.

677 38. Eschenfeldt WH, Lucy S, Millard CS, Joachimiak A, Mark ID. 2009. A family of LIC vectors
678 for high-throughput cloning and purification of proteins. Methods Mol Biol 498:105–115.

679 39. Errey J, Lee S, Gibson R, Fleites C, Barry C, Jung P, O'Sullivan A, Davis B, Davies G. 2010.
680 Mechanistic insight into enzymatic glycosyl transfer with retention of configuration through
681 analysis of glycomimetic inhibitors. Angew Chem Int Ed Engl 49:1234–7.

682 40. Kabsch W. 2010. XDS. Acta Crystallogr D Biol Crystallogr 66:125–132.

683 41. Emsley P, Cowtan K. 2004. Coot: model-building tools for molecular graphics. Acta
684 Crystallogr D Biol Crystallogr 60:2126–2132.

Figure 1

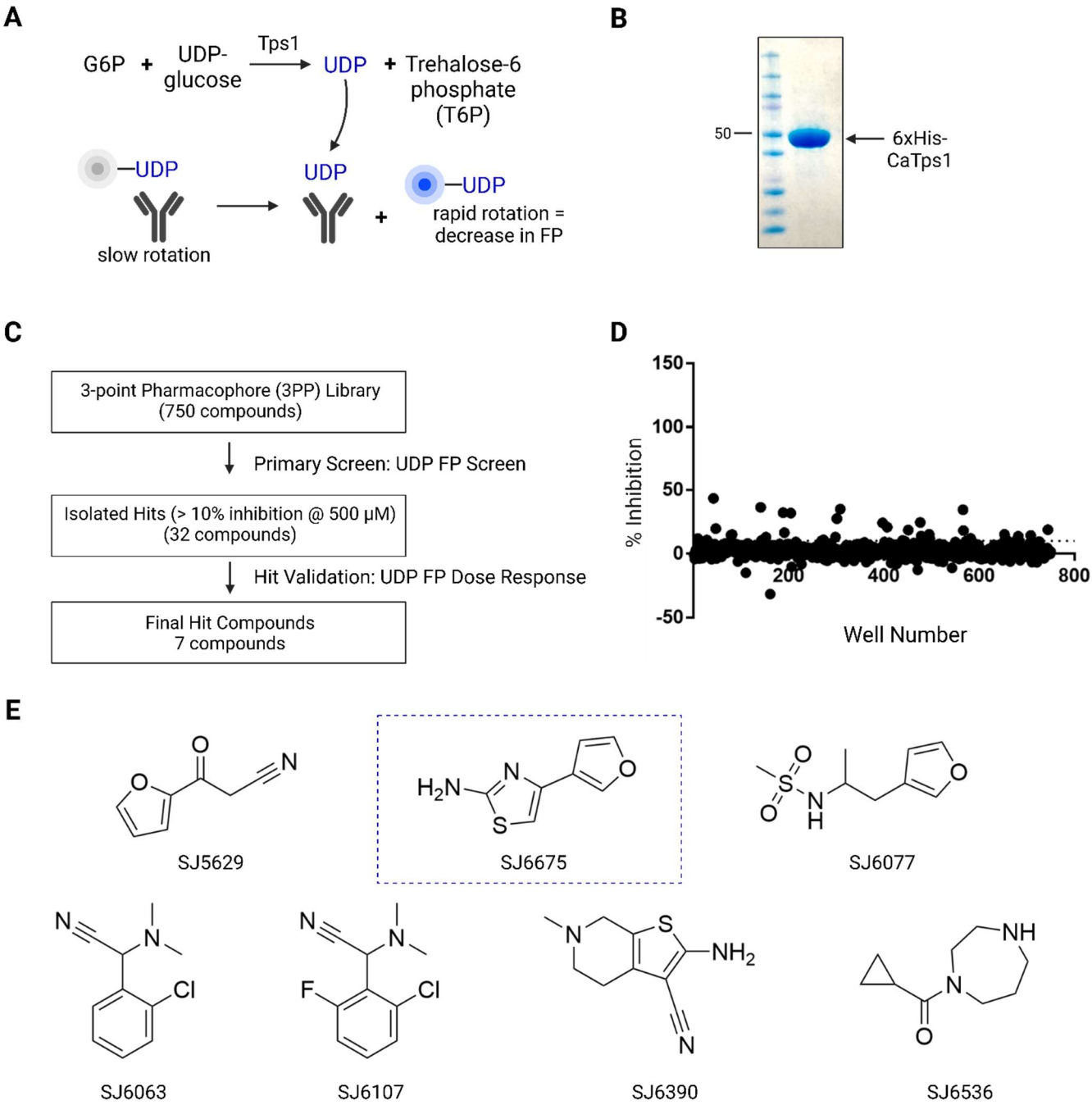
A
G6P + UDP-glucose
Tps1
UDP + Trehalose-6 phosphate (T6P)
UDP
UDP
UDP
slow rotation
rapid rotation = decrease in FP
B
50
6xHis-CaTps1
C
3-point Pharmacophore (3PP) Library (750 compounds)
Primary Screen: UDP FP Screen
Isolated Hits (> 10% inhibition @ 500 μM) (32 compounds)
Hit Validation: UDP FP Dose Response
Final Hit Compounds 7 compounds
D
% Inhibition
150
100
50
0
-50
200
400
600
800
Well Number
E
SJ5629
SJ6675
SJ6077
SJ6063
SJ6107
SJ6390
SJ6536

Figure 2

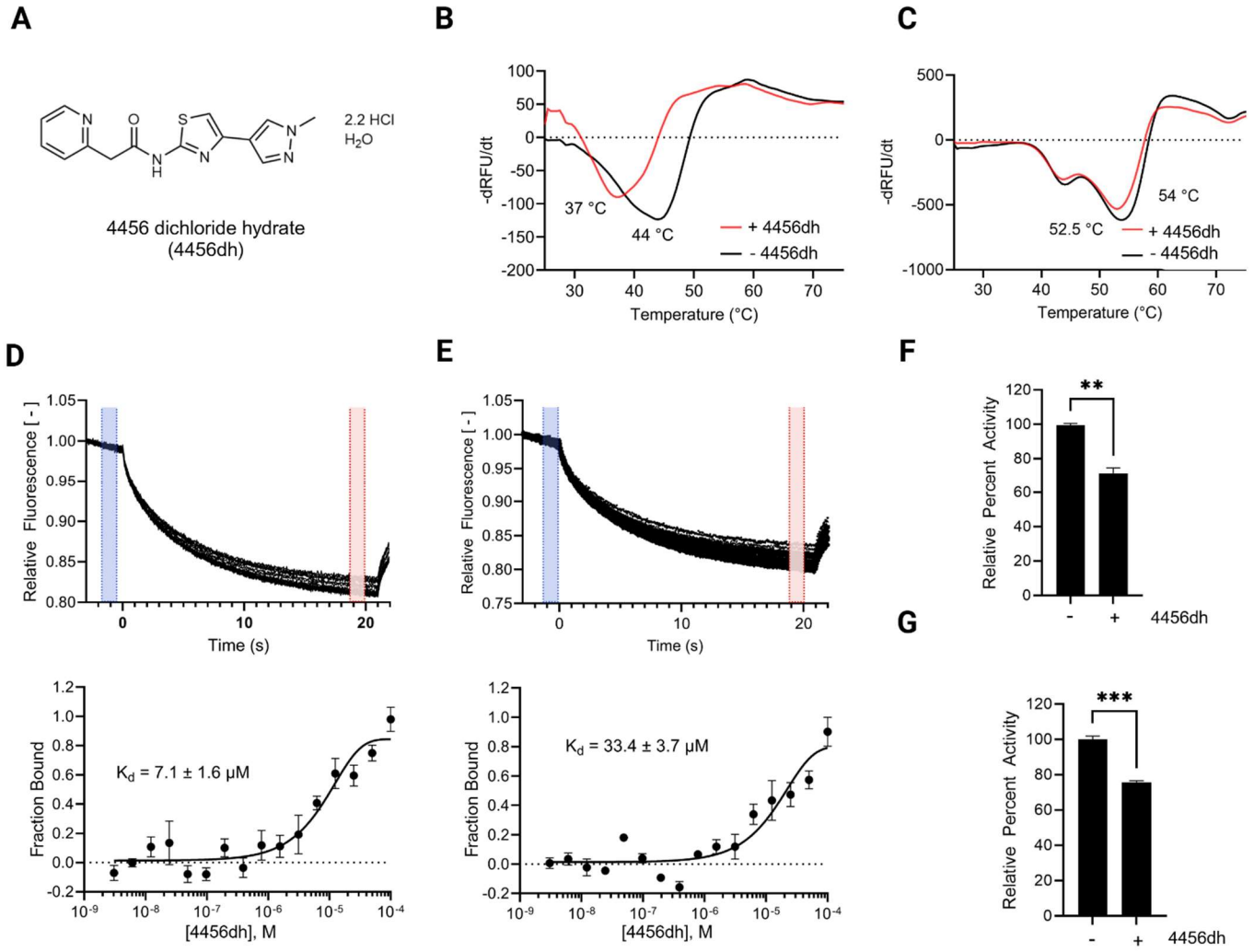
A
2.2 HCl
H_2O
4456 dichloride hydrate
(4456dh)
B
-dRFU/dt
37 °C
44 °C
+ 4456dh
- 4456dh
Temperature (°C)
C
-dRFU/dt
54 °C
52.5 °C
+ 4456dh
- 4456dh
Temperature (°C)
D
Relative Fluorescence [-]
Time (s)
Fraction Bound
K_d = 7.1 ± 1.6 μM
[4456dh], M
E
Relative Fluorescence [-]
Time (s)
Fraction Bound
K_d = 33.4 ± 3.7 μM
[4456dh], M
F
Relative Percent Activity
**
- + 4456dh
G
Relative Percent Activity
***
- + 4456dh

Figure 3

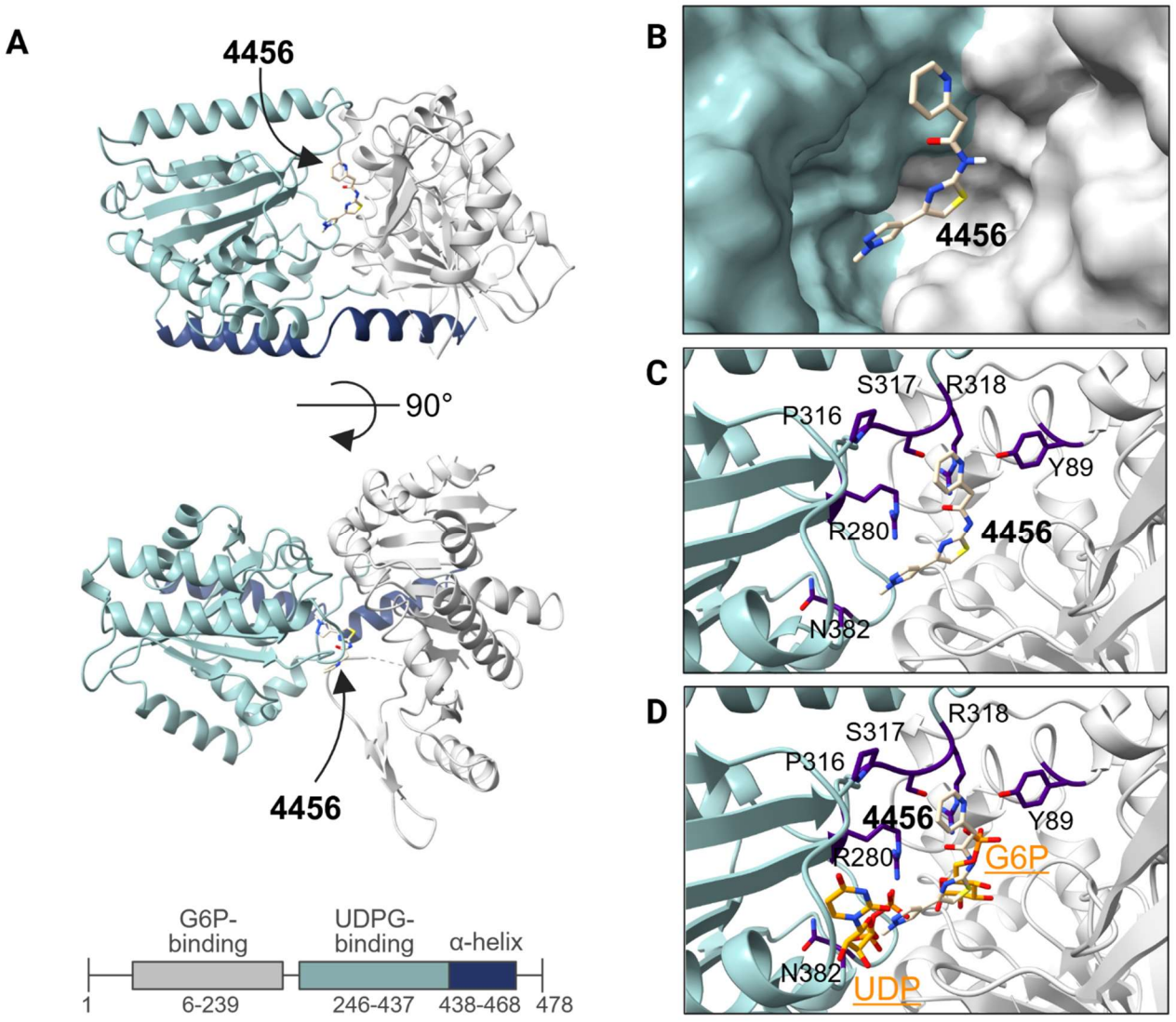
A
4456
90°
4456
G6P-
binding
UDPG-
binding
α-helix
1
6-239
246-437
438-468
478
B
4456
C
S317
R318
P316
Y89
R280
4456
N382
D
R318
S317
P316
4456
Y89
R280
G6P
N382
UDP

Figure 4

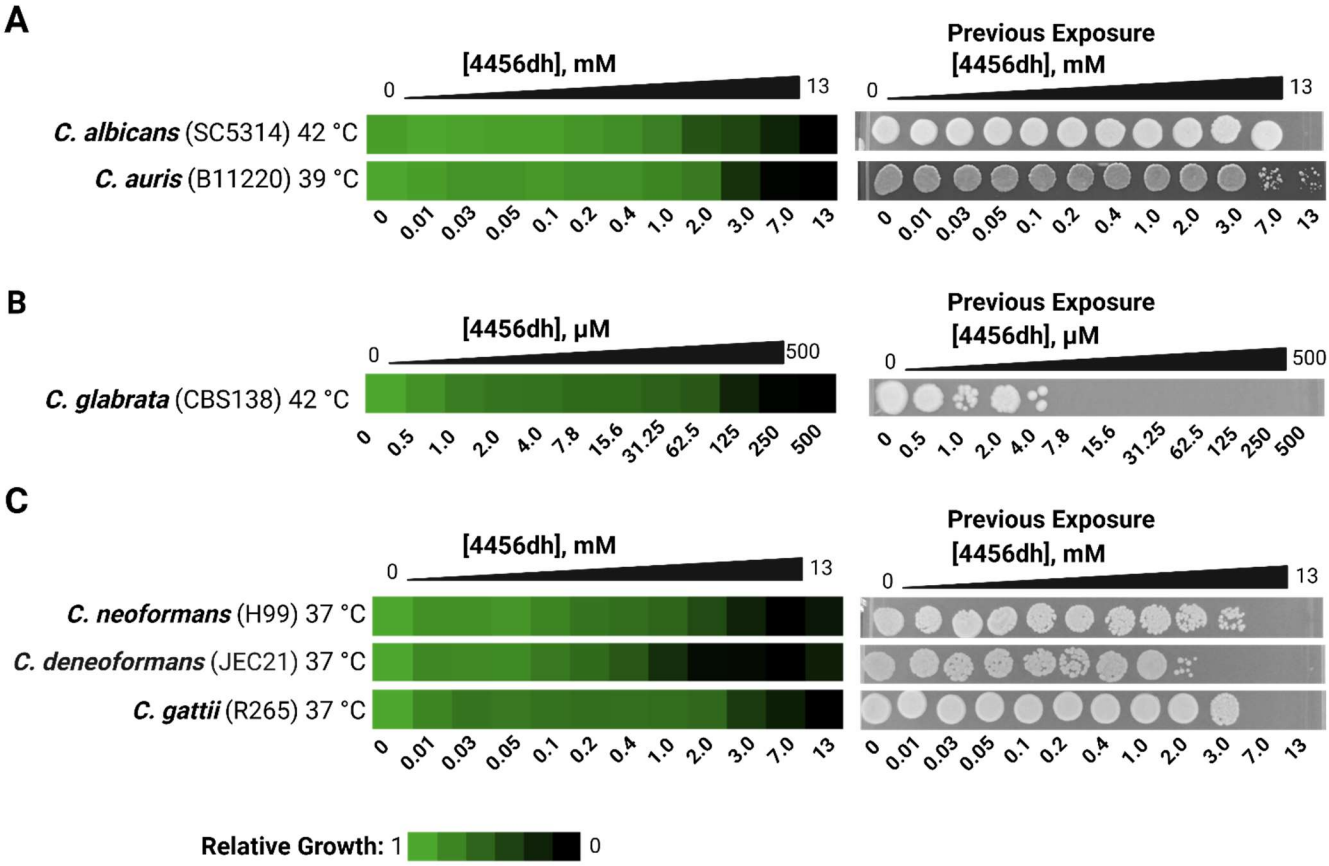
A
[4456dh], mM
0
13
Previous Exposure
[4456dh], mM
0
13
C. albicans (SC5314) 42 °C
C. auris (B11220) 39 °C
0 0.01 0.03 0.05 0.1 0.2 0.4 1.0 2.0 3.0 7.0 13
0 0.01 0.03 0.05 0.1 0.2 0.4 1.0 2.0 3.0 7.0 13
B
[4456dh], µM
0
500
Previous Exposure
[4456dh], µM
0
500
C. glabrata (CBS138) 42 °C
0 0.5 1.0 2.0 4.0 7.8 15.6 31.25 62.5 125 250 500
0 0.5 1.0 2.0 4.0 7.8 15.6 31.25 62.5 125 250 500
C
[4456dh], mM
0
13
Previous Exposure
[4456dh], mM
0
13
C. neoformans (H99) 37 °C
C. deneoformans (JEC21) 37 °C
C. gattii (R265) 37 °C
0 0.01 0.03 0.05 0.1 0.2 0.4 1.0 2.0 3.0 7.0 13
0 0.01 0.03 0.05 0.1 0.2 0.4 1.0 2.0 3.0 7.0 13
Relative Growth: 1
0

Figure 5

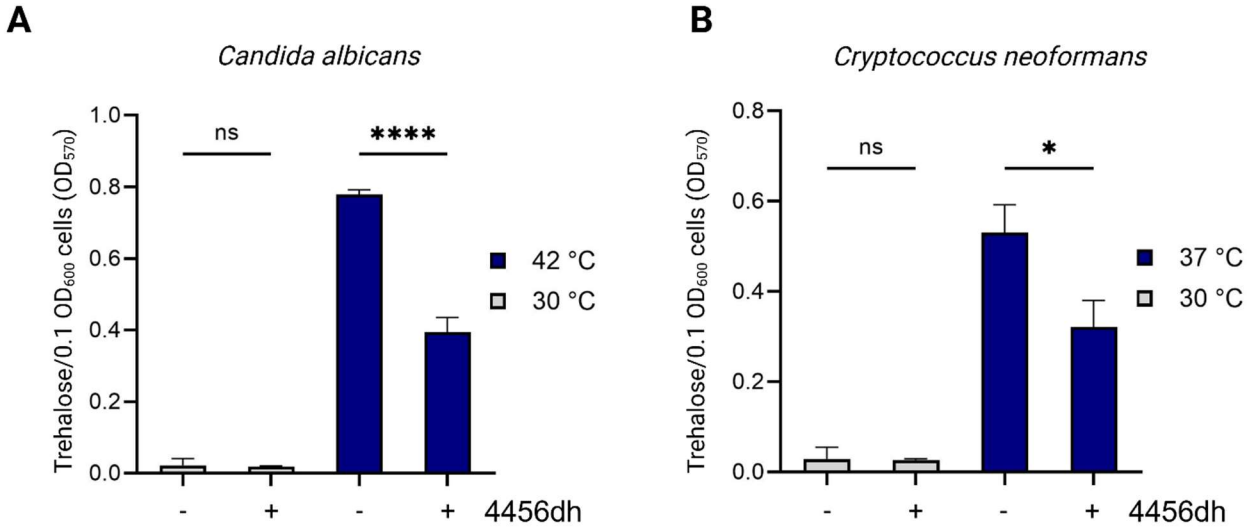
A
Candida albicans
Trehalose/0.1 OD600 cells (OD570)
1.0
0.8
0.6
0.4
0.2
0.0
ns
****
42 °C
30 °C
-
+
-
+
4456dh
B
Cryptococcus neoformans
Trehalose/0.1 OD600 cells (OD570)
0.8
0.6
0.4
0.2
0.0
ns
*
37 °C
30 °C
-
+
-
+
4456dh